JACS
JOURNAL OF THE AMERICAN CHEMICAL SOCIETY
Article
Cite This: J. Am. Chem. Soc. 2019, 141, 13841−13848
pubs.acs.org/JACS

Face-Sharing Archimedean Solids Stacking for the Construction of Mixed-Ligand Metal−Organic Frameworks

Yu-Chen Qiu,[†,⊥] Shuai Yuan,[∥] Xiao-Xin Li,[§] Dong-Ying Du,[‡] Cong Wang,[‡] Jun-Sheng Qin,*[,†,∥,#] Hannah F. Drake,[∥] Ya-Qian Lan,*[,§] Lei Jiang,[†,⊥] and Hong-Cai Zhou*[,∥,∇]

[†]State Key Laboratory of Inorganic Synthesis and Preparative Chemistry, College of Chemistry, Jilin University, Changchun 130012, PR China

[‡]National & Local United Engineering Lab for Power Battery, Department of Chemistry, Northeast Normal University, Changchun 130024, PR China

[§]School of Chemistry and Materials Science, Nanjing Normal University, Nanjing 210023, PR China

[∥]Department of Chemistry, Texas A&M University, College Station, Texas 77843-3255, United States

[⊥]Key Laboratory of Bio-inspired Materials and Interfacial Science, Technical Institute of Physics and Chemistry, Chinese Academy of Sciences, Beijing 100190, PR China

[#]International Center of Future Science, Jilin University, Changchun 130012, PR China

[∇]Department of Materials Science and Engineering, Texas A&M University, College Station, Texas 77843-3003, United States

Supporting Information

ABSTRACT: Reticular chemistry has been an important guiding principle for the design of metal−organic frameworks (MOFs). This approach utilizes discrete building units (molecules and clusters) that are connected through strong bonds into extended networks assisted by topological considerations. Although the simple design principle of connecting points and lines has proved successful, new design strategies are still needed to further explore the structures and functions of MOFs. Herein, we report the design and synthesis of two mixed-ligand MOFs, $[(CH_3)_2NH_2]_4[Zn_4O]_4[Zn(TCPP)]_5[BTB]_{8/3}$ (PCN-137) and $[Zr_6(\mu_3\text{-}O)_4(\mu_3\text{-}OH)_4][TCPP][TBTB]_{8/3}$ (PCN-138) (BTB = 1,3,5-benzene(tris)-benzoate, TBTB = 4,4′,4″-(2,4,6-trimethylbenzene-1,3,5-triyl)tribenzoate, and TCPP = tetrakis(4-carboxyphenyl)porphyrin) by the stacking of face-sharing Archimedean solids. In these two MOFs, high-symmetrical metal clusters serve as vertices, and tritopic or tetratopic carboxylate ligands function as triangular and square faces, leading to the formation of two kinds of Archimedean solids (rhombicuboctahedron and cuboctahedron). Furthermore, the ordered accumulation of Archimedean solids successfully gives rise to 3D structures through face-sharing, highlighting the polyhedron-based approach for the design and preparation of MOFs. In addition, PCN-138 was utilized as a heterogeneous catalyst toward CO_2 photoreduction under visible-light irradiation. This structure shows high photocatalytic activity, which can be attributed to the coexistence of photosensitizing porphyrin fragments and Zr-oxo centers within the PCN-138 scaffold.

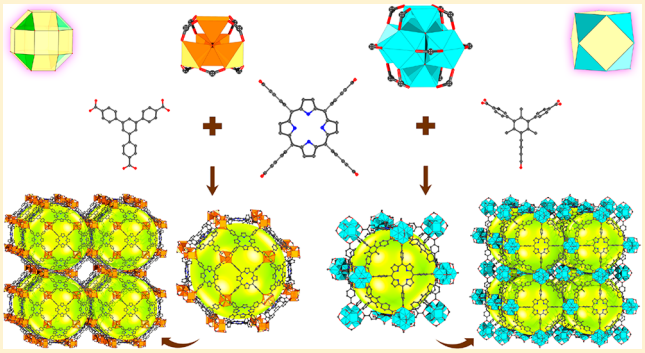

INTRODUCTION

In the past decades, metal−organic materials (MOMs), a class of crystalline materials, have risen to the forefront of solid-state chemistry and material science.[1−5] MOMs provide a high degree of structural and functional tunability by the judicious selection of metal nodes and organic ligands through either one-pot assembly or postsynthetic modifications. These materials have also been demonstrated to be ideal candidates for addressing many enduring societal challenges pertaining to energy and environmental sustainability. Generally, inorganic metal nodes are linked to organic ligands by coordination bonds forming periodic structures. These can range from individual zero-dimensional (0D) metal−organic polyhedra (MOPs) in the case of supramolecules to extended polyhedra in three-dimensional (3D) networks in metal−organic frameworks (MOFs), also known as porous coordination polymers (PCPs). In MOFs, metal nodes serve as the vertices and organic ligands as connectors or edges. Reticular chemistry, proposed by Yaghi and O'Keeffe,[6,7] is the well-interpreted and designed synthesis of MOF materials with targeted porosity, pore size, and functionality by the deconstruction of the

Received: May 24, 2019
Published: July 25, 2019

DOI: 10.1021/jacs.9b05580
J. Am. Chem. Soc. 2019, 141, 13841−13848

structures into their underlying nets (framework topologies).[8−10] In addition, 3D MOF structures can be theoretically generated through the ordered accumulation of geometric polyhedron, in which metal nodes act as the vertices and organic ligands serve as faces.

Convex polyhedra (including Platonic, Archimedean, Kepler and Goldberg polyhedra) are of broad interest for supramolecular chemists owing to their aesthetic beauty and geometric relevance.[11,12] There are some examples of MOP architectures that utilize Platonic (regular) and Archimedean (semiregular) solids in the literature.[13] Platonic solids embody a family of five convex uniform polyhedra that are made of the same regular polygons, whereas Archimedean solids consist of 13 convex polyhedra constructed from at least two different regular polygons that meet at identical vertices. Most MOP systems described in the literature are tetrahedral, cubic, or octahedral ensembles that can be classified as Platonic solids.[3,14−16] For the more complex Archimedean solids, only a few examples have yet been reported.[17−21] In the reported MOPs, however, the metal nodes are regarded as vertices and the organic linkers as edges. In reported MOFs, periodic structures are formed utilizing the basis of Platonic polyhedra with metal nodes as the vertices and organic ligands as edges (Figure S1); such as in the cubic IRMOF series and the octahedral UiO-66 series.[1,6,22] In addition, Archimedean solid accumulation is almost only encountered in zeolitic imidazolate framework (ZIF) family. These structures are constructed from tetrahedral metal ions (e.g., M = Zn or Co) and bridged by imidazolate (Im) linkers.[23,24] The fact that the M−Im−M angle is similar to that of the Si−O−Si angle (145°) means that in zeolites, the formation of four-, six-, and eight-membered rings as squares, hexagons, and octagons of two Archimedean solids is preferred (Figure S2).[25,26] Although Archimedean solids are common in ZIFs, the studies on the accumulation of other Archimedean solids is rarely explored due to the specific synthetic challenges. First, the Archimedean solids possess identical vertices like the Platonic solids in light of geometric symmetry. Second, each member of Archimedean family is made up of at least two different regular polygons. Third, each regular polygon (including the equilateral triangle, square, pentagon, hexagon, octagon, and decagon) in the Archimedean solid must also have edge lengths that are equal. As a result, the rational design and self-assembly of MOF structures with Archimedean polyhedron-blueprints with organic fragments as faces is a challenge in synthetic chemistry. Although this approach has been rarely exploited, it still offers a great potential for the rational design and construction of MOFs.

Archimedean solids consisting of equilateral triangles and squares—cuboctahedron and rhombicuboctahedron (Scheme 1a−d)—possess six squares located at the face-centered cubic lattice. This feature makes it possible for the structures to stack in 3D direction like cubes, but with interspacing (Scheme 1e,f). The organic BTB ligand (or TBTB, BTB = 1,3,5-benzene(tris)benzoate, TBTB = 4,4′,4″-(2,4,6-trimethylbenzene-1,3,5-triyl)tribenzoate) and TCPP ligand (TCPP = tetrakis(4-carboxyphenyl)porphyrin) possess similar side lengths as equilateral triangles and squares, respectively. Given the constrains necessary to synthesize Archimedean solids, BTB (or TBTB) and TCPP were chosen to construct Archimedean polyhedron-based MOPs because of their equivalent edge lengths. On the basis of topological analysis (Scheme 1e,f) of the 3D frameworks with (3,4,7)- and

Scheme 1. Two Kinds of Archimedean Solids That Are Composed of (a) Equilateral Triangles and (b) Squares: (c) Cuboctahedron and (d) Rhombicuboctahedron; Face-Sharing Archimedean Solids Stacking Arrangement in the Construction of Their Respective (e,f) 3D Frameworks

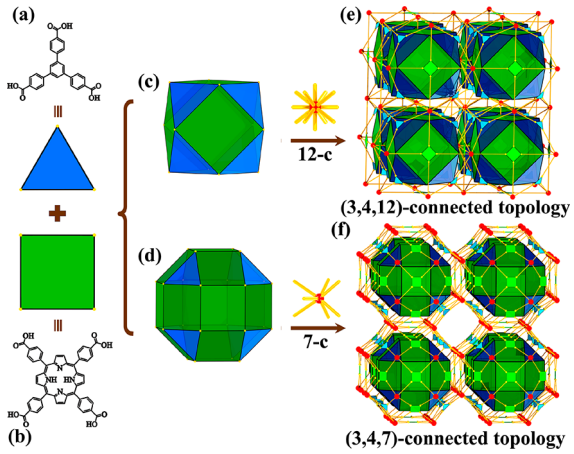

(3,4,12)-connected topologies, it is possible to construct rhombicuboctahedron and cuboctahedron-based cages into MOFs. In this sense, the selection of 7- and 12-connected metal nodes was another key factor for the construction of Archimedean solid-based MOFs. A 7-connected metal node with a high symmetry is very rare in the literature with a 7-connected Zn_4O cluster being one of the few reported.[27] For the 12-connected possibility, Zr_6 cluster was chosen as this cluster is well-known to be an excellent building unit as a result of its exceptional stability and tunable connectivity (from 6 to 12).[28−30] Two MOFs based on Archimedean solids (rhombicuboctahedron and cuboctahedron, respectively), $[(CH_3)_2NH_2]_4[Zn_4O]_4[Zn(TCPP)]_5[BTB]_{8/3}$ (PCN-137) and $[Zr_6(\mu_3\text{-}O)_4(\mu_3\text{-}OH)_4][TCPP][TBTB]_{8/3}$ (PCN-138), were synthesized through geometric accumulation. Herein, we demonstrate a new strategy for the design and synthesis of MOFs based on the face-sharing of convex polyhedron. The nitrogen adsorption−desorption isotherms at 77 K suggested the architectural stability and permanent porosity of the PCN-138 structure. Furthermore, PCN-138 was employed as an effective photocatalyst toward CO_2 reduction in the presence of triisopropanolamine (TIPA) as a sacrificial reagent under visible-light irradiation. PCN-138 was shown to possess efficient photocatalytic activity, which can be attributed to the coexistence of photosensitive porphyrin ligands and Zr-oxo centers in the PCN-138 framework.

■ RESULTS AND DISCUSSION

Structural Design. Conventionally, MOFs are constructed from metal-based units (metal ions or clusters) as nodes and bridging organic ligands as linkers through coordination bonds.[31−33] An analogy to polyhedral systems (either regular or irregular), the metal nodes serve as vertices and bridging organic ligands work as edges. In this way, if organic ligands function as the faces of the polyhedra, ditopic organic linkers should be excluded. This exclusion is because the organic ligands should at a minimum have a triangular shape, with at least three distinct connections. In addition to this requirement, other prerequisites should be satisfied in order to obtain Archimedean polyhedron-based MOFs. First, in light of geometric symmetry, the Archimedean solids must possess

DOI: 10.1021/jacs.9b05580
J. Am. Chem. Soc. 2019, 141, 13841−13848

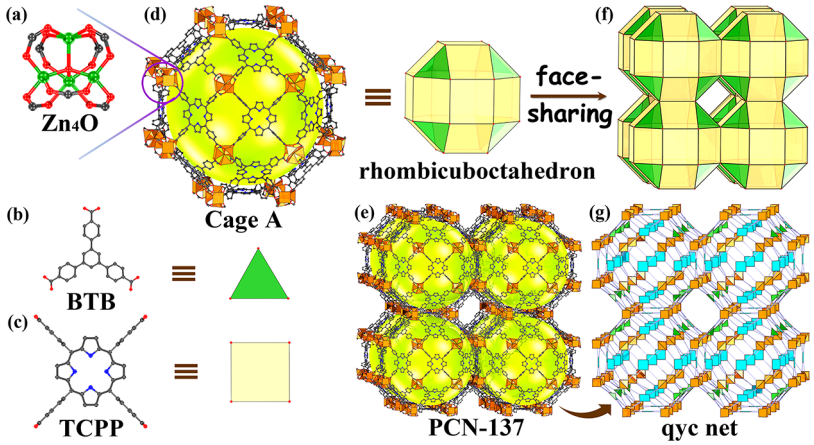

Figure 1. Structure of PCN-137: (a) 7-connected Zn_4O cluster, (b) BTB, and (c) TCPP, (d) the rhombicuboctahedron cage. Face-sharing rhombicuboctahedron stacking (f) for the formation of 3D structure (e) with (3,4,7)-connected topology (g). H atoms are omitted for clarity.

identical vertices, as in Platonic solids. In this sense, there can be only one type of metal-based unit formed in the reaction system. Second, each member of the Archimedean family is made up of at least two different regular polygons. For our purposes, it would be a mixed-ligand system containing at least two kinds of symmetric organic ligands. Third, the edge lengths of the various regular polygons (including the equilateral triangle, square, pentagon, hexagon, octagon, and decagon) must be all equal in each Archimedean solid. In this vein, the organic ligands selected for this study should have similar edge lengths to one another. The synthetic system containing the polytopic organic ligands was hard to crystallize as the system is limited by the solubility and connectivity of the linkers.[34] We attempted to synthesize Archimedean polyhedra from equilateral triangles and squares, generating cuboctahedron and rhombicuboctahedron. These solids can be derived from two Platonic solids (octahedron and cube with O_h symmetry) through trunction and cantellation, respectively.

A rhombicuboctahedron-based MOF, PCN-137, was successfully synthesized from a 7-connected metal cluster, BTB ligand and TCPP ligand through geometric accumulation. However, further trials on the combination of BTB and TCPP ligands in Zr^{IV} salt medium failed to form Archimedean polyhedron-based frameworks. Instead, a layer-pillar structure, PCN-134, was formed. In PCN-134, the connection between the Zr_6 clusters and the BTB moieties formed a (3,6)-connected layer that was further extended into a 3D pillared framework with TCPP fragments.[35] This result was attributed to the BTB ligand which has a greater degree of flexibility in the ligand geometry than other ligand possibilities. In order to meet the angular requirement necessary to form an Archimedean polyhedron-based framework, we attempted to tune the ligand conformation by varying the spacer moieties within the BTB ligand. Following this strategy, a TBTB (4,4′,4″-(2,4,6-trimethylbenzene-1,3,5-triyl)tribenzoate) ligand was utilized instead of the BTB ligand due to the three carboxylate groups in this structure being almost 90° out of plane with the central benzene ring. This ligand geometry angle results from steric hindrance from the presence of the three methyl groups.[36,37] After exchanging the BTB ligand for the TBTB ligand in the synthetic process, PCN-138 was generated through cuboctahedron accumulation.

Structural Description. Single-crystal X-ray diffraction studies reveal that PCN-137 crystallized in the cubic space group $Pm\bar{3}m$ (No. 221, Table S1). The asymmetric unit in the framework of this structure contained unique Zn1 and Zn2 atoms with 1/2 and 1/2 occupancy factors, respectively, a central oxygen atom with a 1/4 occupancy factor, two square planar [ZnTCPP] fragments with 1/4 and 1/16 occupancy factors, and a triangular planar BTB ligand with a 1/6 occupancy factor. The Zn1 centers were completed by three carboxylate-based oxygen atoms and one central μ_4-O atom, whereas the Zn2 centers were coordinated to four carboxylate-based oxygen atoms and one central μ_4-O atom. The central μ_4-oxygen atom was connected to two Zn1 and two Zn2 atoms forming the $Zn_4(\mu_4\text{-O})$ cluster (Figure 1a). This cluster was coordinated to seven carboxylate groups (five from [ZnTCPP] moieties and two from BTB ligands) forming a 7-connected node (Figure S3). Unlike the well-known 6-connected $[Zn_4O(COO)_6]$ cluster observed in the classical IRMOF-*n* series and other compounds,[1,6] two Zn atoms exhibited tetrahedral coordination geometries and two Zn atoms adopted a five-coordinate trigonal bipyramid geometry in the PCN-137 framework (Figure S4). Such a connectivity mode is very unusual and, to the best of our knowledge, very few examples of 7-connected Zn_4O clusters have ever been reported.[27,38] As expected, 18 TCPP and 8 BTB fragments were connected through 24 Zn_4O clusters generating a regular rhombicuboctahedron cage with O_h symmetry (Figure 1d). This result was owed to the similar distances of the carboxylate groups between the two rigid ligands, BTB and TCPP (Figure 1b,c). The tritopic and tetratopic ligands (BTB and TCPP) in the structure functioned as the faces of Archimedean solid, while the Zn_4O clusters functioned as the vertices. In the literature, there was a very common cage constructed by 12 dimetal paddlewheel clusters and 24 isophthalate structural moieties.[18] Connecting the 12 dimetal clusters forms a cuboctahedron,[39] while linking the 24 isophthalate moieties gives rise to a rhombicuboctahedron.[40,41] The difference was that the isophthalate moieties for the ligand produced a rhombicuboctahedron with an open window and fixed sizes for the edges of the polyhedron. This was in contrast to the TCPP and BTB ligands located in the faces of the rhombicuboctahedron cage in the PCN-137 structure (Figure S5). On the surface of each rhombicuboctahedron (Figure S6), there were two types of faces: 18 square faces and 8 triangular faces, each with side lengths of ∼18.0 Å (the centroid−centroid distances of two neighboring Zn_4O clusters). The internal diameter for

DOI: 10.1021/jacs.9b05580
J. Am. Chem. Soc. 2019, 141, 13841−13848

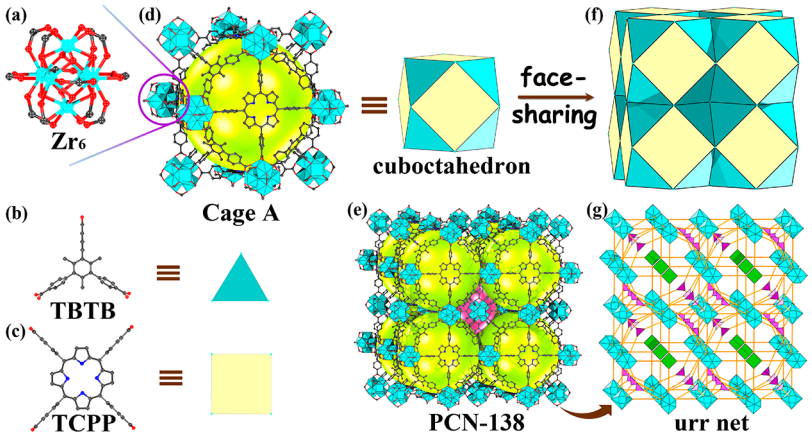

Figure 2. Structure of PCN-138: (a) 12-connected Zr_6 cluster, (b) TBTB, and (c) TCPP, (d) the cuboctahedron cage. Face-sharing cuboctahedron stacking (f) for the formation of 3D structure (e) with (3,4,12)-connected topology (g). H atoms are omitted for clarity.

the resulting rhombicuboctahedron cage was ∼40 Å (Figure S7), which is an unusually large cavity among reported MOFs.[42] In addition, eight BTB ligands were connected through 12 Zn_4O clusters generating the first cage, a cuboctahedron cage, with six open square windows. The other cage in the structure was generated from four TCPP ligands linked to eight Zn_4O clusters forming a cube with two open square windows (Figure S8). The internal diameters for the resulted cuboctahedron and cube cages were ∼24 and ∼18 Å (excluding van der Waals radii), respectively. Furthermore, each cuboctahedron was connected to six adjacent cubes and eight adjacent rhombicuboctahedrons through face-sharing, forming the three-dimensional network of PCN-137 (Figure 1e,f and S9). In the PCN-137 structure, the ratio of rhombicuboctahedrons/cuboctahedrons/cubes was 1:1:3. Each tetratopic porphyrin TCPP fragment was connected to four Zn_4O clusters which acted as 4-connected nodes. Each tritopic BTB ligand was bound to three Zn_4O clusters serving as a 3-connected node. In each case, each carboxylic group in the ligand was bound to only one Zn_4O cluster. Such connectivity leads to an extended 3D framework with an ideal (3,4,7)-connected topology, namely **qyc** (Figure 1g). After further analysis of the (3,4,7)-connected topology, the topology of the structure is derived from the combination of the **rhr-b** and **tfe** topologies (Figure S10).[9,43] The anionic framework of PCN-137 was balanced by $[(CH_3)_2NH_2]^+$ cations, which was generated through the well-established decarbonylation of DMA upon heating around or over 100 °C.[44] And this phenomenon was commonly occurred in the previous work.[45,46]

A single-crystal X-ray diffraction study on the structure of PCN-138 revealed that it crystallized into a cubic crystal system with a $Pm\bar{3}m$ space group (No. 221, Table S1). In the asymmetric unit, there were two unique Zr1 and Zr2 atoms with 1/4 and 1/8 occupancy factors, square TCPP ligands with a 1/16 occupancy factor, and triangular TBTB ligand with a 1/6 occupancy factor. The $[Zr_6(\mu_3\text{-O})_4(\mu_3\text{-OH})_4(COO)_{12}]$ (Zr_6, Figure 2a) cluster exhibited a classic 12-connected model identical to the clusters in the UiO-type structures (UiO stands for University of Oslo).[22] Each Zr_6 cluster was connected to four distinct TCPP ligands in the equatorial plane (*ab*-plane or *ac*-plane) through four carboxylate groups and eight TBTB ligands above and below the equatorial plane through eight carboxylate groups (Figures 2b,c and S11). In turn, each deprotonated TBTB or TCPP ligand was interlinked three or four Zr_6 clusters, respectively. Such connectivity leads to the formation of two cages with different sizes in the PCN-138 framework. The first cage was derived from eight triangular TBTB and six square TCPP moieties bridged by a total of 12 Zr_6 clusters, forming a large nanoscale cuboctahedron with O_h symmetry and a diameter of ∼26 Å (Figures 2d and S12). The centroid−centroid distance between two adjacent Zr_6 clusters was ∼19 Å. In the second cage, eight TBTB ligands were shown to connect each other through six Zr_6 clusters, giving rise to a small octahedron with O_h symmetry (Figure S13). The internal diameter for the resulting octahedron was 16 Å (excluding van der Waals radii, Figure S14). In the structure, the octahedral cages connected to the cuboctahedron cages formed a 3D network of PCN-138 with a cuboctahedron/octahedron ratio of 1:1. In this arrangement, each octahedral cage was surrounded by eight neighboring cuboctahedron cages through face-sharing (Figures 2e,f and S15). From this viewpoint, each Zr_6 cluster could be simplified into a 12-connected node, and the TBTB and TCPP ligands could be regarded as 3- and 4-connected nodes. As a result, the overall framework of PCN-138 was a 3D (3,4,12)-connected **urr** net (Figure 2g).

As for the TCPP ligands utilized in PCN-137 and PCN-138, the four terminal phenyl rings were all perpendicular to the inner central porphyrin ring (Figures S5, S16 and Table S2). The dihedral angles between the central benzene ring and the terminal benzoic acid fragments in the BTB ligand were ∼5.9° in PCN-137. Meanwhile, the dihedral angles between the central benzene ring and the terminal benzoic acid fragments in the TBTB ligand were 90° in PCN-138. The C−C bonds of the TCPP and BTB (TBTB) ligands were able to rotate freely between the terminal benzoic acid arms and the central porphyrin or benzene core to generate a nonplanar conformation. It may be this rotational freedom in the ligands that aided in the construction of these 3D cage-based MOFs (PCN-137 and -138). In order to confirm our deduction, the conformations of the TCPP and BTB ligands in PCN-134 were also analyzed because of the composition similarities between PCN-138 and PCN-134.[35] The dihedral angles between the central porphyrin ring and the terminal benzoic acid fragments in the TCPP ligands were 88.659° in PCN-134; which was close to the angle for the ligand seen in PCN-138. However, the dihedral angles of the central benzene ring and the terminal benzoic acid fragments in the BTB ligand in PCN-134 were 25.858°, 26.169°, and 26.169°, respectively. This is

DOI: 10.1021/jacs.9b05580
J. Am. Chem. Soc. 2019, 141, 13841−13848

vastly different than the angles seen in the PCN-138 structure. The steric hindrance effect resulting from the presence of the methyl groups played a critical role in the formation of the dihedral angles of 90° in the TBTB ligand, and therefore the final formation of PCN-138.

The powder X-ray diffraction (PXRD) patterns of the as-synthesized samples matched well with the simulated patterns (Figures S17 and S18); suggesting the phase purities of PCN-137 and PCN-138. As shown in the thermogravimetric analysis (TGA) curves (Figure S19), the first continuous weight loss of these two MOFs stepping from room temperature to ∼200 °C corresponds to the loss of all solvent molecules. PCN-137 and PCN-138 begin to decompose at temperature higher than ∼400 °C or ∼380 °C, respectively. The calculated solvent accessible volume of PCN-138 was as large as 68.7% according to the calculations using PLATON.[47] The N_2 adsorption−desorption isotherms of PCN-138 at 77 K showed a reversible type-I isotherm (Figure S20), confirming the architectural stability and permanent porosity of PCN-138. The Brunauer−Emmett−Teller (BET) surface area, calculated from nitrogen sorption results for PCN-138, was 1261 $m^2 \cdot g^{-1}$. In addition, the CO_2 adsorption−desorption isotherms of PCN-138 were measured at 273 and 298 K (described in Figure S21). The isotherms showed the carbon dioxide uptake to be as high as 63.07 and 40.72 $cm^3\ g^{-1}$ at saturation, respectively, which is helpful for the study of CO_2 conversion.[48−50]

Photoelectrochemical Properties. As indicated by the UV−vis measurements, PCN-138 demonstrated a broad-band absorption in the visible light region up to 680 nm (Figure 3a). Absorption at this wavelength is desirable for photocatalytic applications. The optical absorption of PCN-138 could be attributed to the absorption features of the free TCPP ligand.[48] This result suggested that the electrons in the PCN-138 structure could be easily promoted from a lower energy state to an excited state upon visible-light irradiation. Furthermore, the photocurrent curve of PCN-138 also indicated that this MOF was active under visible light illumination (Figure 3b). In order to elucidate possible semiconductor characteristics present in PCN-138, a series of Mott−Schottky experiments were carried out at frequencies of 500, 1000, and 1500 Hz. As shown in Figure 3c, the positive slope of the experimental C^{-2} values (vs the applied potentials) agreed with those of typical n-type semiconductors. In the study, the intersection point was independent of the frequency, and the flat band position of ∼ −1.06 V vs Ag/AgCl was determined from the intersection (that is, −0.86 V vs Normal Hydrogen Electrode (NHE)). The bottom of the conduction band (the lowest unoccupied molecular orbital (LUMO)) in a n-type semiconductors is approximately equal to the flat-band potential.[51] According to this, the LUMO of PCN-138 could be estimated to be −0.86 V vs NHE. On the basis of the UV−vis diffuse reflectance data, the optical bandgap of PCN-138 was calculated to be 1.82 eV (Figure S22). The valence band (the highest occupied molecular orbital (HOMO)) of PCN-138 was also estimated to be 0.96 V vs NHE (Figure 3c, insert). It is theoretically feasible for the reduction of CO_2 to be accomplished using PCN-138 as a photocatalyst. This reduction was possible due to the negative potential of the LUMO in PCN-138 relative to the reduction potential for the conversion of CO_2 to formate (−0.28 V vs NHE). In order to improve the preciseness, ultraviolet photoelectron spectroscopy (UPS) of PCN-138 was carried out to determine the position of valence band and verify the correctness of band gap structure (Figure S23). The

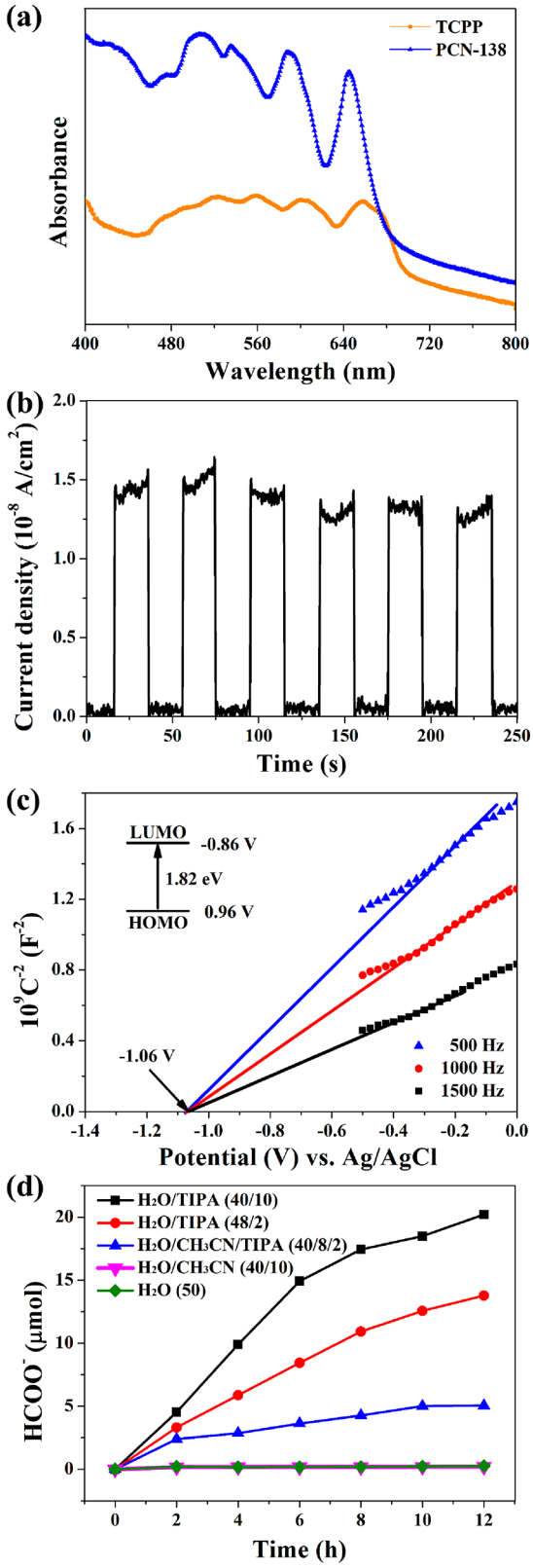

Figure 3. (a) UV−vis spectra of PCN-138 and TCPP. (b) Transient photocurrent response of PCN-138 in 0.5 M Na_2SO_4 aqueous solution under visible light irradiation. (c) Mott−Schottky plots for PCN-138 in 0.2 M Na_2SO_4 aqueous solution; inset is the energy diagram of the HOMO and LUMO levels of PCN-138. (d) The amounts of $HCOO^-$ produced as a function of irradiation time with PCN-138 as photocatalysts (10 mg). solvent, 50 mL; Xe light (300 W, $\lambda \geq 420$ nm).

DOI: 10.1021/jacs.9b05580
J. Am. Chem. Soc. 2019, 141, 13841−13848

band gap of PCN-138 is calculated to be 1.78 eV, which is very close to that obtained from Tauc's plot.

Furthermore, the electronic properties of PCN-138 were investigated by calculating the band structure and partial density of states (PDOS) using density functional theory (DFT). PCN-138 is a semiconductor with the band gap of 1.85 eV from the DFT calculations (Figure S24). The PDOS analysis further indicates that the valence band is mainly contributed by C 2p and O 2p states and slightly contributed by Zr 3d states, and the conduction band is dominantly contributed by C 2p states and minority from O 2p states. The Bader charge of Zr in PCN-138 is +2.53 |e|. All these data suggest that the electronic properties of PCN-138 is mainly derived from the organic moieties. This result is in agreement with the UV−vis analysis that the absorption peaks of PCN-138 and TCPP are close (Figure 3a), suggesting that it is $\pi-\pi$ transitions on the ligand.

Photocatalytic Reduction of CO_2. Given the broad absorption in the visible light region and the semiconductor of PCN-138, the reduction of carbon dioxide was evaluated by utilizing PCN-138 as a photocatalyst. This reduction was performed in the presence of triisopropanolamine (TIPA). In the reaction setup, TIPA was employed as an electron donor and as a hydrogen donor to for the recyclability of the catalytic process. TIPA was used in this study as it provided a milder alkaline environment than triethanolamine (TEOA). The visible-light-driven photoreduction of CO_2 by employing PCN-138 as a photocatalyst was studied under reaction conditions otherwise described in the literature. Control experiments were designed to investigate the photocatalytic reaction. The concentration of $HCOO^-$ anions in the reaction were detected and quantitatively analyzed by ion chromatography in situ. The results showed a time-dependent increase of product under continuous visible-light illumination (Figure 3d). The results suggested that few formate anions were produced when the reaction occurred in the absence of TIPA in either a single solvent (water) or a mixed solvent system (H_2O/MeCN). PCN-138 was demonstrated to show higher photocatalytic activity for carbon dioxide reduction in water medium than in a mixed H_2O/MeCN system in the presence of TIPA. Moreover, the ratio of H_2O (solvent) and TIPA (sacrificial agent) was also shown to play an important role in the formate product yield. As shown in Figure 3d, an amount of 20.21 μmol formate anions was able to be produced within 12 h in a water media (40 mL), in the presence of TIPA (10 mL), under continuous Xe light illumination (300 W, $\lambda \geq 420$ nm). No other products were detected in the gas or liquid phases, suggesting that PCN-138 was highly selective toward this conversion as a photocatalyst. It is notable that PCN-138 exhibited one of the highest performances of visible-light-driven CO_2 photoreduction to formate among the reported MOFs or crystalline photocatalysts.[48,49] As a control, TCPP was utilized as a photocatalyst under the same conditions. Free TCPP ligand showed no activity toward CO_2 as a photoreductant. These results suggested that the photocatalytic activity exhibited by the PCN-138 system could be greatly improved in the MOF form over that of the free TCPP ligand. In addition, PCN-138, as heterogeneous catalyst, can be easily separated and recovered from the reaction media by centrifugation for continued use. The recyclability performance of PCN-138 was further investigated to examine its long-term activity and stability. The results suggested that PCN-138 could be reused for the photoreduction of CO_2 without an obvious decrease in the MOF activity during four continuous runs (Figure S25). After the fourth photocatalytic experiment, the PXRD pattern demonstrated that the structural integrity of PCN-138 was maintained (Figure S18).

Furthermore, electron paramagnetic resonance (EPR) studies were also carried out to detect the electron transfer pathway as well as to determine the active catalytic species during the photocatalytic reaction. As shown in Figure S26, when the sample (PCN-138 + TIPA) under N_2 was irradiated with visible light, a strong EPR signal at $g = 2.0033$ attributed to Zr^{III} could be observed. It is believed that Zr^{III}, was generated by an electron transfer from the excited state of the organic linker to the Zr-oxo clusters in a ligand to metal charge transfer under visible-light irradiation.[52,53] When CO_2 was introduced into the irradiated system, the Zr^{III} EPR signal intensity became weaker. This result could be explained through the electrons being further transferred to CO_2 from Zr^{III} metal centers. As a result, Zr^{III} is partially oxidized back to Zr^{IV} resulting in a loss of intensity in the signal. These results indicated that the photogenerated Zr^{III} was involved during the photocatalytic CO_2 reduction.

Through the observation of the experimental results, a reasonable reaction mechanism for the photocatalytic reduction of carbon dioxide was discerned for PCN-138 (Figure S27). The large cage within the PCN-138 framework endows the structure to readily adsorb carbon dioxide. When the reaction system was irradiated, the TCPP ligand generated photoelectrons which were transferred to the Zr-oxo clusters. The metal centers in the clusters were reduced from Zr^{IV} to Zr^{III}, facilitating the reduction of carbon dioxide to $HCOO^-$ and simultaneously oxidizing the Zr^{III} metal centers back to Zr^{IV}.[48,54] When tested, the TCPP ligand did not show any activity for the photocatalytic reduction of CO_2, suggesting that the framework itself played an important role in the photoreduction process.

■ CONCLUSIONS

In conclusion, two mixed-ligand Archimedean polyhedron-based MOFs (PCN-137 and PCN-138) were synthesized based on polyhedron-blueprints. From the structural viewpoint, the metal clusters served as vertices and the polytopic carboxylate ligands functioned as faces of the polyhedron in these two MOFs. Furthermore, the ordered accumulation of Archimedean solids (rhombicuboctahedron and cuboctahedron) successfully constructed the 3D structures of PCN-137 and PCN-138 through face-sharing. As a heterogeneous catalyst, PCN-138 exhibited a highly efficient photocatalytic activity toward CO_2 reduction under visible-light irradiation owing to its broad absorption in the visible light region, the semiconductor characteristics and high CO_2 uptake. The present work not only demonstrates a successful case for the construction of mixed-ligand Archimedean polyhedron-based MOFs, but it also offers an efficient photocatalyst with excellent activity. Moreover, the polyhedron-blueprint strategy in this study provided for the possibility of new ways of thinking about the design of solid-state MOMs. More investigations into the myriad of polyhedron-based design options are currently underway in our lab.

■ ASSOCIATED CONTENT

Supporting Information

The Supporting Information is available free of charge on the ACS Publications website at DOI: 10.1021/jacs.9b05580.

DOI: 10.1021/jacs.9b05580
J. Am. Chem. Soc. 2019, 141, 13841−13848

Text and tables giving experimental procedures for the preparation of PCN-137 and PCN-138, photocatalytic CO_2 reduction, DFT calculations, PXRD patterns, gas adsorption isotherms, and other additional information (PDF)

X-ray crystallographic details of PCN-137 (CIF)

X-ray crystallographic details of PCN-138 (CIF)

■ AUTHOR INFORMATION

Corresponding Authors

*qin@jlu.edu.cn
*yqlan@njnu.edu.cn
*zhou@chem.tamu.edu

ORCID

Shuai Yuan: 0000-0003-3329-0481
Jun-Sheng Qin: 0000-0003-2531-552X
Ya-Qian Lan: 0000-0002-2140-7980
Lei Jiang: 0000-0003-4579-728X
Hong-Cai Zhou: 0000-0002-9029-3788

Notes

The authors declare no competing financial interest.

■ ACKNOWLEDGMENTS

This work was supported by the Center for Gas Separations Relevant to Clean Energy Technologies, an Energy Frontier Research Center funded by the U.S. Department of Energy, Office of Science, Office of Basic Energy Sciences (DE-SC0001015). The authors also acknowledge financial support from the National Natural Science Foundation of China (Grant Nos. 21621001 and 21673036) and the 111 Project (Grant No. B17020). The authors also acknowledge financial support from U.S. Department of Energy, Office of Fossil Energy, National Energy Technology Laboratory (DE-FE0026472). This work was also funded by the Robert A. Welch Foundation through a Welch Endowed Chair to HJZ (A-0030). The National Science Foundation Small Business Innovation Research (NSF-SBIR, No. 1632486) and National Science Foundation Graduate Research Fellowship (DGE: 1252521) are gratefully acknowledged. We thank Dr. Min Zhang for valuable discussions on DFT calculations and Dr. Mian Li for topological analysis.

■ REFERENCES

(1) Li, H.; Eddaoudi, M.; O'Keeffe, M.; Yaghi, O. M. Design and synthesis of an exceptionally stable and highly porous metal-organic framework. *Nature* **1999**, *402*, 276−279.

(2) Kitaura, R.; Fujimoto, K.; Noro, S.; Kondo, M.; Kitagawa, S. A pillared-layer coordination polymer network displaying hysteretic sorption: Cu-2(pzdc)(2)(dpyg) (n) (pzdc = pyrazine-2,3-dicarboxylate; dpyg = 1,2-di(4-pyridyl)glycol). *Angew. Chem., Int. Ed.* **2002**, *41* (1), 133−135.

(3) Perry, J. J. t.; Perman, J. A.; Zaworotko, M. J. Design and synthesis of metal-organic frameworks using metal-organic polyhedra as supermolecular building blocks. *Chem. Soc. Rev.* **2009**, *38* (5), 1400−1417.

(4) Furukawa, H.; Cordova, K. E.; O'Keeffe, M.; Yaghi, O. M. The Chemistry and Applications of Metal-Organic Frameworks. *Science* **2013**, *341* (6149), 1230444.

(5) Kitagawa, S. Future Porous Materials. *Acc. Chem. Res.* **2017**, *50* (3), 514−516.

(6) Eddaoudi, M.; Kim, J.; Rosi, N.; Vodak, D.; Wachter, J.; O'Keeffe, M.; Yaghi, O. M. Systematic Design of Pore Size and Functionality in Isoreticular MOFs and Their Application in Methane Storage. *Science* **2002**, *295* (5554), 469−472.

(7) Yaghi, O. M.; O'Keeffe, M.; Ockwig, N. W.; Chae, H. K.; Eddaoudi, M.; Kim, J. Reticular synthesis and the design of new materials. *Nature* **2003**, *423* (6941), 705−714.

(8) O'Keeffe, M.; Yaghi, O. M. Deconstructing the Crystal Structures of Metal-Organic Frameworks and Related Materials into Their Underlying Nets. *Chem. Rev.* **2012**, *112* (2), 675−702.

(9) Li, M.; Li, D.; O'Keeffe, M.; Yaghi, O. M. Topological Analysis of Metal-Organic Frameworks with Polytopic Linkers and/or Multiple Building Units and the Minimal Transitivity Principle. *Chem. Rev.* **2014**, *114* (2), 1343−1370.

(10) Schoedel, A.; Li, M.; Li, D.; O'Keeffe, M.; Yaghi, O. M. Structures of Metal-Organic Frameworks with Rod Secondary Building Units. *Chem. Rev.* **2016**, *116* (19), 12466−12535.

(11) MacGillivray, L. R.; Atwood, J. L. Structural Classification and General Principles for the Design of Spherical Molecular Hosts. *Angew. Chem., Int. Ed.* **1999**, *38* (8), 1018−1033.

(12) Senechal, M. *Shaping Space: Exploring Polyhedra in Nature, Art, and the Geometrical Imagination*; Springer Science & Business Media, 2013.

(13) MacGillivray, L. R. Design rules: a net and Archimedean polyhedra score big for self-assembly. *Angew. Chem., Int. Ed.* **2012**, *51* (5), 1110−1112.

(14) Enemark, E. J.; Stack, T. D. P. Stereospecificity and Self-Selectivity in the Generation of a Chiral Molecular Tetrahedron by Metal-Assisted Self-Assembly. *Angew. Chem., Int. Ed.* **1998**, *37* (7), 932−935.

(15) Heinrich, J. L.; Berseth, P. A.; Long, J. R. Molecular Prussian Blue analogues: synthesis and structure of cubic $Cr_4Co_4(CN)_{12}$ and $Co_8(CN)_{12}$ clusters. *Chem. Commun.* **1998**, 1231−1232.

(16) Suzuki, K.; Tominaga, M.; Kawano, M.; Fujita, M. Self-assembly of an M_6L_{12} coordination cube. *Chem. Commun.* **2009**, 1638−1640.

(17) Leininger, S.; Fan, J.; Schmitz, M.; Stang, P. J. Archimedean solids: transition metal mediated rational self-assembly of supramolecular-truncated tetrahedra. *Proc. Natl. Acad. Sci. U. S. A.* **2000**, *97* (4), 1380−1384.

(18) Eddaoudi, M.; Kim, J.; Wachter, J. B.; Chae, H. K.; O'Keeffe, M.; Yaghi, O. M. Porous Metal−Organic Polyhedra: 25 Å Cuboctahedron Constructed from 12 $Cu_2(CO_2)_4$ Paddle-Wheel Building Blocks. *J. Am. Chem. Soc.* **2001**, *123* (18), 4368−4369.

(19) Tominaga, M.; Suzuki, K.; Kawano, M.; Kusukawa, T.; Ozeki, T.; Sakamoto, S.; Yamaguchi, K.; Fujita, M. Finite, spherical coordination networks that self-organize from 36 small components. *Angew. Chem., Int. Ed.* **2004**, *43* (42), 5621−5625.

(20) Ni, Z.; Yassar, A.; Antoun, T.; Yaghi, O. M. Porous metal-organic truncated octahedron constructed from paddle-wheel squares and terthiophene links. *J. Am. Chem. Soc.* **2005**, *127* (37), 12752−12753.

(21) Sun, Q. F.; Iwasa, J.; Ogawa, D.; Ishido, Y.; Sato, S.; Ozeki, T.; Sei, Y.; Yamaguchi, K.; Fujita, M. Self-assembled $M_{24}L_{48}$ polyhedra and their sharp structural switch upon subtle ligand variation. *Science* **2010**, *328* (5982), 1144−1147.

(22) Cavka, J. H.; Jakobsen, S.; Olsbye, U.; Guillou, N.; Lamberti, C.; Bordiga, S.; Lillerud, K. P. A new zirconium inorganic building brick forming metal organic frameworks with exceptional stability. *J. Am. Chem. Soc.* **2008**, *130* (42), 13850−13851.

(23) Phan, A.; Doonan, C. J.; Uribe-Romo, F. J.; Knobler, C. B.; O'Keeffe, M.; Yaghi, O. M. Synthesis, structure, and carbon dioxide capture properties of zeolitic imidazolate frameworks. *Acc. Chem. Res.* **2010**, *43* (1), 58−67.

(24) Tan, Y. X.; Wang, F.; Zhang, J. Design and synthesis of multifunctional metal-organic zeolites. *Chem. Soc. Rev.* **2018**, *47* (6), 2130−2144.

(25) Park, K. S.; Ni, Z.; Cote, A. P.; Choi, J. Y.; Huang, R.; Uribe-Romo, F. J.; Chae, H. K.; O'Keeffe, M.; Yaghi, O. M. Exceptional chemical and thermal stability of zeolitic imidazolate frameworks. *Proc. Natl. Acad. Sci. U. S. A.* **2006**, *103* (27), 10186−10191.

DOI: 10.1021/jacs.9b05580
J. Am. Chem. Soc. 2019, 141, 13841−13848

(26) Hayashi, H.; Cote, A. P.; Furukawa, H.; O'Keeffe, M.; Yaghi, O. M. Zeolite A imidazolate frameworks. *Nat. Mater.* **2007**, *6* (7), 501−506.
(27) He, W. W.; Li, S. L.; Yang, G. S.; Lan, Y. Q.; Su, Z. M.; Fu, Q. Controllable synthesis of a non-interpenetrating microporous metal-organic framework based on octahedral cage-like building units for highly efficient reversible adsorption of iodine. *Chem. Commun.* **2012**, *48* (80), 10001−10003.
(28) Bai, Y.; Dou, Y. B.; Xie, L. H.; Rutledge, W.; Li, J. R.; Zhou, H. C. Zr-based metal-organic frameworks: design, synthesis, structure, and applications. *Chem. Soc. Rev.* **2016**, *45* (8), 2327−2367.
(29) Rimoldi, M.; Howarth, A. J.; DeStefano, M. R.; Lin, L.; Goswami, S.; Li, P.; Hupp, J. T.; Farha, O. K. Catalytic Zirconium/Hafnium-Based Metal−Organic Frameworks. *ACS Catal.* **2017**, *7* (2), 997−1014.
(30) Yuan, S.; Qin, J. S.; Lollar, C. T.; Zhou, H. C. Stable Metal-Organic Frameworks with Group 4 Metals: Current Status and Trends. *ACS Cent. Sci.* **2018**, *4* (4), 440−450.
(31) Guillerm, V.; Weselinski, L.; Belmabkhout, Y.; Cairns, A. J.; D'Elia, V.; Wojtas, L.; Adil, K.; Eddaoudi, M. Discovery and introduction of a (3,18)-connected net as an ideal blueprint for the design of metal-organic frameworks. *Nat. Chem.* **2014**, *6* (8), 673−680.
(32) Kalmutzki, M. J.; Hanikel, N.; Yaghi, O. M. Secondary building units as the turning point in the development of the reticular chemistry of MOFs. *Sci. Adv.* **2018**, *4* (10), No. eaat9180.
(33) Liu, Q.; Song, Y.; Ma, Y.; Zhou, Y.; Cong, H.; Wang, C.; Wu, J.; Hu, G.; O'Keeffe, M.; Deng, H. Mesoporous Cages in Chemically Robust MOFs Created by a Large Number of Vertices with Reduced Connectivity. *J. Am. Chem. Soc.* **2019**, *141* (1), 488−496.
(34) Lu, W. G.; Wei, Z. W.; Gu, Z. Y.; Liu, T. F.; Park, J.; Park, J.; Tian, J.; Zhang, M. W.; Zhang, Q.; Gentle, T.; Bosch, M.; Zhou, H. C. Tuning the structure and function of metal-organic frameworks via linker design. *Chem. Soc. Rev.* **2014**, *43* (16), 5561−5593.
(35) Yuan, S.; Qin, J. S.; Zou, L. F.; Chen, Y. P.; Wang, X.; Zhang, Q.; Zhou, H. C. Thermodynamically Guided Synthesis of Mixed-Linker Zr-MOFs with Enhanced Tunability. *J. Am. Chem. Soc.* **2016**, *138* (20), 6636−6642.
(36) Zhao, X.; He, H.; Dai, F.; Sun, D.; Ke, Y. Supramolecular isomerism in honeycomb metal-organic frameworks driven by CH···pi interactions: homochiral crystallization from an achiral ligand through chiral inducement. *Inorg. Chem.* **2010**, *49* (19), 8650−8652.
(37) Liu, T.-F.; Vermeulen, N. A.; Howarth, A. J.; Li, P.; Sarjeant, A. A.; Hupp, J. T.; Farha, O. K. Adding to the Arsenal of Zirconium-Based Metal-Organic Frameworks: the Topology as a Platform for Solvent-Assisted Metal Incorporation. *Eur. J. Inorg. Chem.* **2016**, *2016* (27), 4349−4352.
(38) Zhang, M. W.; Chen, Y. P.; Zhou, H. C. Structural design of porous coordination networks from tetrahedral building units. *CrystEngComm* **2013**, *15* (45), 9544−9552.
(39) Wang, H. N.; Meng, X.; Yang, G. S.; Wang, X. L.; Shao, K. Z.; Su, Z. M.; Wang, C. G. Stepwise assembly of metal-organic framework based on a metal-organic polyhedron precursor for drug delivery. *Chem. Commun.* **2011**, *47* (25), 7128−7130.
(40) Zhao, D.; Yuan, D.; Sun, D.; Zhou, H. C. Stabilization of metal-organic frameworks with high surface areas by the incorporation of mesocavities with microwindows. *J. Am. Chem. Soc.* **2009**, *131* (26), 9186−9188.
(41) Yuan, D.; Zhao, D.; Sun, D.; Zhou, H. C. An isoreticular series of metal-organic frameworks with dendritic hexacarboxylate ligands and exceptionally high gas-uptake capacity. *Angew. Chem., Int. Ed.* **2010**, *49* (31), 5357−5361.
(42) Zhuang, W.; Ma, S.; Wang, X.-S.; Yuan, D.; Li, J.-R.; Zhao, D.; Zhou, H.-C. Introduction of cavities up to 4 nm into a hierarchically-assembled metal−organic framework using an angular, tetratopic ligand. *Chem. Commun.* **2010**, *46* (29), 5223−5225.
(43) Delgado Friedrichs, O.; O'Keeffe, M.; Yaghi, O. M. Three-periodic nets and tilings: semiregular nets. *Acta Crystallogr., Sect. A: Found. Crystallogr.* **2003**, *59*, 515−525.
(44) Wan, Y.; Alterman, M.; Larhed, M.; Hallberg, A. Dimethylformamide as a Carbon Monoxide Source in Fast Palladium-Catalyzed Aminocarbonylations of Aryl Bromides. *J. Org. Chem.* **2002**, *67* (17), 6232−6235.
(45) Xue, D. X.; Cairns, A. J.; Belmabkhout, Y.; Wojtas, L.; Liu, Y.; Alkordi, M. H.; Eddaoudi, M. Tunable rare-earth fcu-MOFs: a platform for systematic enhancement of CO_2 adsorption energetics and uptake. *J. Am. Chem. Soc.* **2013**, *135* (20), 7660−7667.
(46) Qin, J. S.; Du, D. Y.; Li, M.; Lian, X. Z.; Dong, L. Z.; Bosch, M.; Su, Z. M.; Zhang, Q.; Li, S. L.; Lan, Y. Q.; Yuan, S.; Zhou, H. C. Derivation and Decoration of Nets with Trigonal-Prismatic Nodes: A Unique Route to Reticular Synthesis of Metal-Organic Frameworks. *J. Am. Chem. Soc.* **2016**, *138* (16), 5299−5307.
(47) Spek, A. L. Single-crystal structure validation with the program PLATON. *J. Appl. Crystallogr.* **2003**, *36* (1), 7−13.
(48) Xu, H. Q.; Hu, J.; Wang, D.; Li, Z.; Zhang, Q.; Luo, Y.; Yu, S. H.; Jiang, H. L. Visible-Light Photoreduction of CO_2 in a Metal-Organic Framework: Boosting Electron-Hole Separation via Electron Trap States. *J. Am. Chem. Soc.* **2015**, *137* (42), 13440−13443.
(49) Chen, D.; Xing, H.; Wang, C.; Su, Z. Highly efficient visible-light-driven CO_2 reduction to formate by a new anthracene-based zirconium MOF via dual catalytic routes. *J. Mater. Chem. A* **2016**, *4* (7), 2657−2662.
(50) Qin, J. S.; Yuan, S.; Zhang, L.; Li, B.; Du, D. Y.; Huang, N.; Guan, W.; Drake, H. F.; Pang, J.; Lan, Y. Q.; Alsalme, A.; Zhou, H. C. Creating Well-Defined Hexabenzocoronene in Zirconium Metal-Organic Framework by Postsynthetic Annulation. *J. Am. Chem. Soc.* **2019**, *141* (5), 2054−2060.
(51) Maeda, K.; Sekizawa, K.; Ishitani, O. A polymeric-semiconductor−metal-complex hybrid photocatalyst for visible-light CO_2 reduction. *Chem. Commun.* **2013**, *49* (86), 10127−10129.
(52) Long, J.; Wang, S.; Ding, Z.; Wang, S.; Zhou, Y.; Huang, L.; Wang, X. Amine-functionalized zirconium metal-organic framework as efficient visible-light photocatalyst for aerobic organic transformations. *Chem. Commun.* **2012**, *48* (95), 11656−11658.
(53) Zhang, H.; Wei, J.; Dong, J.; Liu, G.; Shi, L.; An, P.; Zhao, G.; Kong, J.; Wang, X.; Meng, X.; Zhang, J.; Ye, J. Efficient Visible-Light-Driven Carbon Dioxide Reduction by a Single-Atom Implanted Metal-Organic Framework. *Angew. Chem., Int. Ed.* **2016**, *55* (46), 14310−14314.
(54) Sun, D.; Fu, Y.; Liu, W.; Ye, L.; Wang, D.; Yang, L.; Fu, X.; Li, Z. Studies on Photocatalytic CO_2 Reduction over NH_2-UiO-66(Zr) and Its Derivatives: Towards a Better Understanding of Photocatalysis on Metal−Organic Frameworks. *Chem. - Eur. J.* **2013**, *19* (42), 14279−14285.

DOI: 10.1021/jacs.9b05580
J. Am. Chem. Soc. 2019, 141, 13841−13848